PHYSICAL REVIEW B **80**, 085406 (2009)

Stacking domains of epitaxial few-layer graphene on SiC(0001)

H. Hibino,[1] S. Mizuno,[2] H. Kageshima,[1] M. Nagase,[1] and H. Yamaguchi[1]
[1]*NTT Basic Research Laboratories, NTT Corporation, Atsugi, Kanagawa 243-0198, Japan*
[2]*Department of Molecular and Material Sciences, Kyushu University, Kasuga, Fukuoka 816-8580, Japan*
(Received 10 April 2009; revised manuscript received 29 June 2009; published 6 August 2009)

We used low-energy electron microscopy (LEEM) and scanning tunneling microscopy (STM) to investigate domain structures of epitaxial few-layer graphene grown on SiC(0001). Dark-field (DF) LEEM images formed using (10) and (01) beams clearly indicate that bilayer graphene consists of two types of domains, which have threefold symmetry and are rotated by 180° with respect to each other. The DF LEEM images show clear domain contrasts at energies where (10)- and (01)-beam intensities calculated for bulk graphite are largely different. This means that the two types of domains are different in stacking: *AB* and *AC* stackings. The stacking domains are also supported by the STM images of bilayer graphene showing both hexagonal and honeycomb patterns.

DOI: 10.1103/PhysRevB.80.085406 PACS number(s): 68.37.Nq, 81.07.−b, 68.55.−a

I. INTRODUCTION

Recently, few-layer graphene (FLG) has attracted much attention as a material for future electronics.[1] Epitaxial FLG fabricated by the thermal decomposition of SiC (Ref. 2) is easily scaled up and promising for device integration. However, because the electronic properties of epitaxial FLG depend on the number of graphene layers,[3–8] the device applications require a reproducible way of forming large-scale graphene layers with an intended thickness. For this purpose, we have already demonstrated that the number of layers in epitaxial FLG can be determined from quantized oscillations of electron reflectivity in low-energy electron microscopy (LEEM).[9–11] Recently there has been some progress in the control of the uniformity of epitaxial graphene,[12–14] to which microscopic evaluation of the number of graphene layers using LEEM has greatly contributed.

While synthesis methods for epitaxial FLG are being intensively studied, the electronic transport properties are also being investigated by several groups.[15–19] FLG grows on both Si-face SiC(0001) and C-face SiC($000\bar{1}$) substrates but there are some differences in its properties between the Si face and C face. It is easier to control the FLG thickness on the Si face than on the C face.[20] The interactions between FLG and the substrate can open a semiconductor gap in FLG on the Si face.[3,5] Therefore, epitaxial FLG grown on the Si face seems more suitable for transistor operations.[18,19] However, epitaxial FLG grown on the Si face so far has much lower mobility than not only FLG exfoliated from bulk graphite but also epitaxial FLG on the C face.[1,15–19] To use epitaxial FLG on the Si face as an electronic material, we have to clarify the reasons for the lower mobility. For this purpose, we are investigating differences in structure between real epitaxial FLG grown on the SiC(0001) Si face and ideal FLG by LEEM and scanning tunneling microscopy (STM). In this paper, we show, using dark-field (DF) imaging of LEEM and calculation of intensity vs energy (*I-V*) curves of low-energy electron-diffraction (LEED) beams, that epitaxial FLG equal to or thicker than a bilayer consists of domains different in stacking order. We also identify stacking structures specific to the domain boundary.

II. EXPERIMENT

The epitaxial FLG was grown on 6H- and 4H-SiC(0001) by annealing the samples at 1300–1500 °C in a commercial LEEM instrument (Elmitec LEEM III). In our LEEM instrument, the electron gun and sample were biased at around 20 kV. The bias difference between the electron gun and sample is normally called the start voltage V_{ST} and eV_{ST} is roughly equal to the electron-beam energy.[8] The number of graphene layers was microscopically determined using the quantized oscillation in the electron reflectivity.[9–11] We also used a commercial STM instrument (Omicron VT-STM) to investigate atomic structures of FLG. The samples were taken out of the LEEM chamber and transferred to the STM chamber in air. After introducing the samples into UHV, we annealed them above 500 °C to remove adsorbates. To determine the stacking orders of bilayer graphene, LEED *I-V* curves were calculated using a Barbieri-Van Hove-symmetrized automated tensor LEED package.[21] The calculated *I-V* curves were shifted in energy by −10 eV to fit the experimental data.

III. RESULTS AND DISCUSSION

Figure 1 shows bright-field (BF) and DF LEEM images of epitaxial FLG grown on 4H-SiC(0001). Figure 1(a) is the BF LEEM image. Numbers in the image denote the number of graphene layers and the surface is mainly covered with bilayer graphene. Figures 1(b)–1(e) are DF LEEM images obtained using (10) and (01) beams at V_{ST}=44.5 and 58.1 V. These images show that graphene equal to or thicker than a bilayer consists of two types of domains. Their contrast is reversed between the (10) and (01) DF LEEM images and also between the DF images of the respective beams taken at V_{ST}=44.5 and 58.1 V. The DF LEEM images using the different beams indicate that the domains have threefold symmetry. Faint linear contrasts in Fig. 1(a) correspond to substrate steps. Figure 1 shows that some domains are continuous across the steps as well as across the boundaries between the bilayer and trilayer.

The two types of domains with threefold symmetry suggest that they are different in the stacking order of graphene

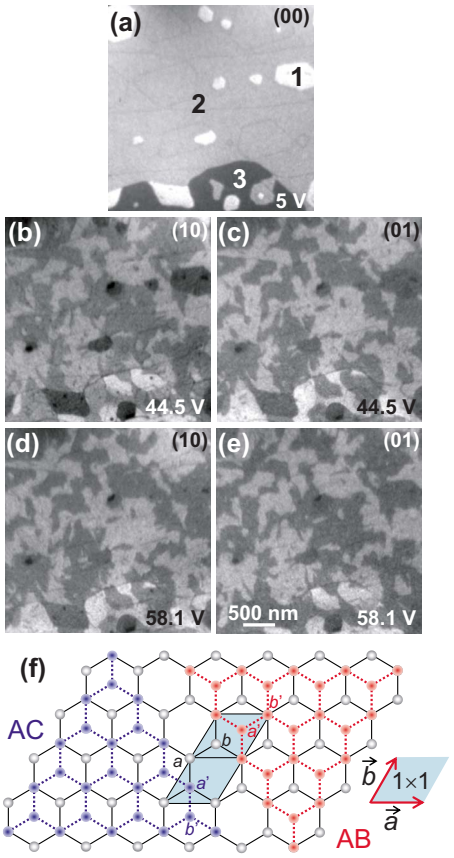

FIG. 1. (Color online) (a) BF LEEM and [(b)–(e)] DF LEEM images of epitaxial FLG grown on 4H-SiC(0001). (f) Schematic illustrations of bilayer graphene with *AB* and *AC* stackings. Numbers in (a) denote the number of graphene layers. Images (b) and (d) are DF LEEM images obtained using the (10) beam, and (c) and (e) are those using the (01) beam. The start voltages were (a) 5 V, [(b) and (c)] 44.5 V, and [(d) and (e)] 58.1 V.

layers. Bilayer graphene has the two types of stacking shown in Fig. 1(f). Carbon atoms occupy *a* and *b* sites in a unit cell of graphene. In bilayer graphene, the *b′* sites in the top layer locate on top of the *a* sites of the bottom layer (called *AB* stacking hereafter) or the *a′* sites in the top layer locate on top of the *b* sites of the bottom layer (*BA* stacking, which is usually called *AC* stacking). *AB* and *AC* stackings both have threefold symmetry and are rotated by 180° with respect to each other.

To confirm that the domains seen in the DF LEEM images originate from the difference in the stacking order, we calculated the LEED *I-V* curves for bulk graphite. To prove the validity of the LEED *I-V* analysis, we first compare the eV_{ST} dependence of the BF LEEM intensity with the calculated LEED *I-V* curve of the (00) beam. In Fig. 2, the BF LEEM intensity for bilayer graphene is plotted as a function of eV_{ST}. Although we calculated this *I-V* curve for bulk graphite with the *ABAB* Bernal stacking without any structural optimizations, the calculated *I-V* curve reproduces the eV_{ST} dependence of the BF LEEM image intensity fairly well at around 40–150 eV. The topmost couple of graphene layers determines the main features in the LEED *I-V* curve. As the energy decreases to less than around 40 eV, the calculated *I-V*

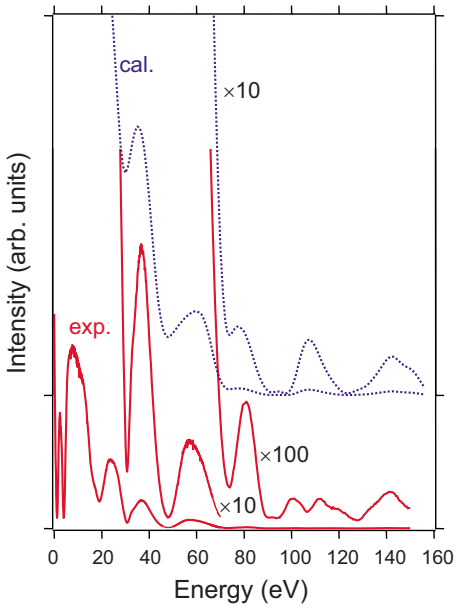

FIG. 2. (Color online) eV_{ST} dependence of the BF LEEM intensity from bilayer graphene (solid line) and LEED *I-V* curve of the (00) beam calculated for bulk graphite with *ABAB* Bernal stacking (dotted line).

curve rapidly increases and deviates from the experiment. This is probably because our calculation procedure did not consider the electronic band structure of graphite at all. Strocov *et al.*[22,23] have already included band structures in the calculations of electron transmission and have succeeded in reproducing the very low-energy electron-diffraction results.

When we obtained the DF LEEM images using the (10) and (01) beams, the incident electron beam was inclined so as to let the diffracted beam come out normally from the surface. We compare the eV_{ST} dependence of the (10) and (01) DF LEEM image intensities with *I-V* curves of the (10) and (01) beams calculated under the normal incidence. From the viewpoint of elastic scattering, these two processes are time-reversed ones and should provide the same diffraction intensity. We have already measured the eV_{ST} dependence of the (10)- and (01)-beam intensities from Si(111)$\sqrt{3}\times\sqrt{3}$-B under the DF LEEM imaging conditions.[24] The measured eV_{ST} dependence of the LEED intensities for the (10) and (01) beams under the normal incidence agreed well with the eV_{ST} dependence of the DF LEEM image intensities.[24] Figure 3 shows the eV_{ST} dependence of the DF LEEM image intensities along with calculated *I-V* curves for the (10) and (01) beams. Because bilayer graphene consists of two types of domains with threefold symmetry, measuring the (10) and (01) DF LEEM image intensities for each type of domain is equivalent to measuring the (10) or (01) DF LEEM image intensities for both types. The experimental data in Fig. 3 were obtained in the latter way. The calculated LEED *I-V* curves reproduce the main features seen in the eV_{ST} dependence. They indicate that the (10) and (01) beams are largely different in intensity at around 45 and 60 eV, which agrees with the clear domain contrasts in Figs. 1(b)–1(e) obtained at 44.5 and 58.1 eV. This means that the domains seen in the DF LEEM images of bilayer graphene have different stacking orders, i.e., *AB* and *AC* stackings.

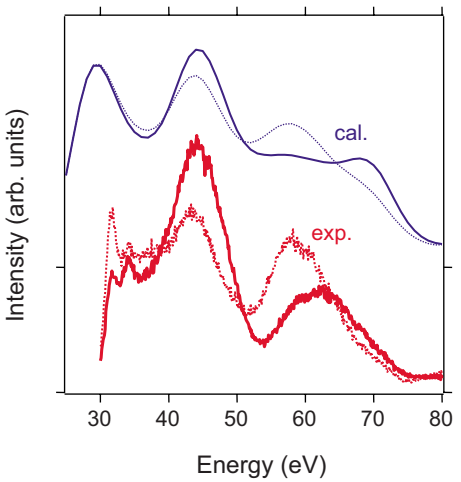

FIG. 3. (Color online) eV_{ST} dependence of the DF LEEM image intensities and calculated LEED *I-V* curves for the (10) and (01) beams. Solid and dotted lines correspond to the (10) and (01) beams, respectively. The calculated LEED *I-V* curves are shifted upward for clarity.

Next, we investigate the boundary structure of the stacking domains. We found that the domain boundaries are visible at certain start voltages in both BF and DF LEEM images. Figures 4(a) and 4(b) are DF LEEM images obtained using the (10) beam at V_{ST}=51.4 and 77.6 V, respectively. In these images, we cannot see all parts of the domain boundaries. The DF LEEM images obtained using (01) and (−11) beams, respectively, make the other parts of the domain boundaries visible, indicating that there are three types of domain boundaries. There are three translation vectors between the *AB* and *AC* stackings, which should correspond to the observed three types of boundaries.

The boundaries should have intermediate structures between the *AB* and *AC* stackings, which are converted by shifting one of the layers in the bilayer relatively to the other. Here, we consider two boundary structures induced by such shifts along high-symmetric directions. When the top layer in *AB* stacking is shifted by $2(\vec{a}+\vec{b})/3$, where $\vec{a}$ and $\vec{b}$ are unit-cell vectors of FLG, *AA* stacking appears between the *AB* and *AC* stackings. The other shift vector we consider is $-(\vec{a}+\vec{b})/3$. This shift causes the boundary structure schematically illustrated in Fig. 4(c) midway from the *AB* to *AC* stacking. Hereafter, we call this type of stacking a shifted stacking.

Figure 4(d) shows calculated LEED *I-V* curves of (10) and (01) beams for bulk graphite with *ABAB* stacking, *AAAA* stacking, and the shifted stacking. Because the *AAAA* stacking has a sixfold symmetry, the (10) and (01) beams have the same intensity. This means that *AA* stacking is inconsistent with the observed three types of boundary structures. However, Lauffer *et al.*[25] observed areas of bilayer graphene whose STM images rather resemble monolayer graphene and suggested that a stacking close to *AA* stacking (which they called *AA′*) could account for the observed images. We suppose that *AA′* stacking provides *I-V* curves similar to *AA* stacking. Therefore, calculated results for *AAAA* stacking are also shown. In the shifted boundary structure, two carbon

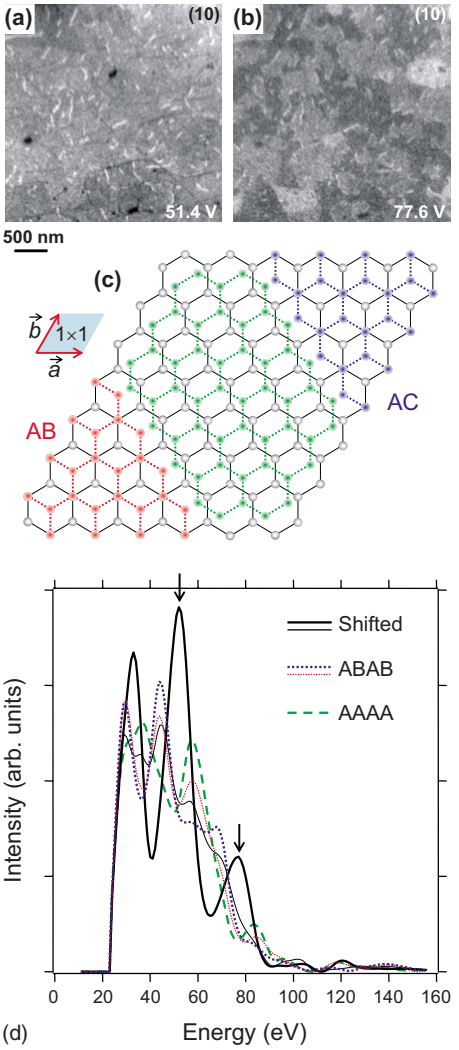

FIG. 4. (Color online) [(a) and (b)] DF LEEM images using the (10) beam at V_{ST}=51.4 and 77.6 V, respectively. The same regions as in Figs. 1(b)–1(e) were imaged. (c) Schematic illustration of the boundary structure with the shifted stacking. (d) LEED *I-V* curves of (10) and (01) beams calculated for bulk graphite with the shifted stacking (solid lines), *ABAB* stacking (dotted lines), and *AAAA* stacking (dashed lines). Thick and thin lines, respectively, correspond to the (10) and (01) beams.

atoms of one layer are located inside the hexagonal ring of the other layer. The two carbon atoms are allowed to align in three directions, resulting in three types of shifted stackings. Each stacking has two mirror planes orthogonal to each other. Therefore, the (10) and (−10) beams are equivalent and the (01), (−11), (0–1), and (1,−1) beams are equivalent too.

In Fig. 4(d), we indicate the start voltages used to obtain Figs. 4(a) and 4(b) by arrows. These start voltages agree with the peak positions of the LEED *I-V* curve for the shifted stacking. On the other hand, *AA* and *AB* stackings should provide similar intensities at these start voltages. *AA* stacking is also inconsistent with the fact that there are three types of domain boundaries. Thus, we conclude that the shifted stacking appears at the boundaries of the stacking domains. We also confirmed that the start voltages at which the boundaries

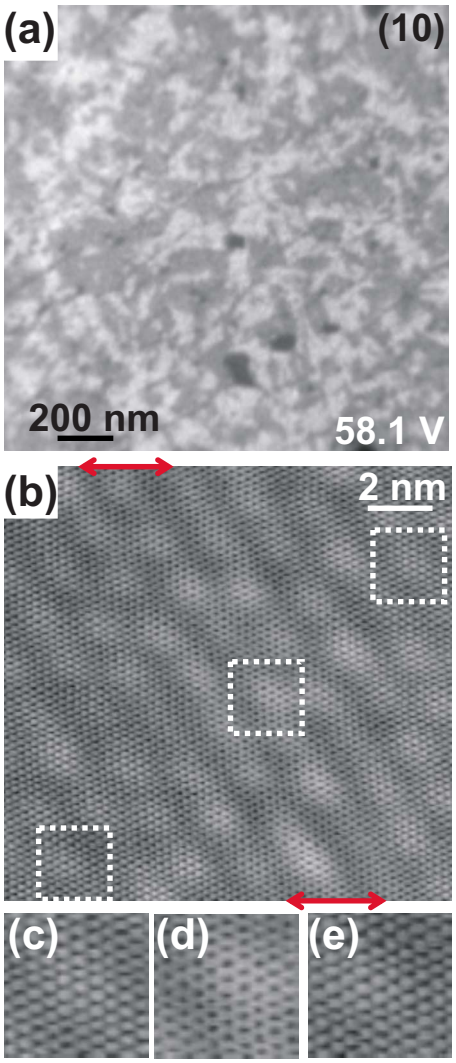

FIG. 5. (Color online) (a) DF LEEM using the (10) beam of epitaxial FLG with the average thickness of bilayer. The start voltage was 58.1 V. (b) STM image of bilayer graphene. [(c)–(e)] Magnified STM images of areas in the dotted squares in (b). The sample bias was −0.18 V.

make contrast in the BF LEEM images are consistent with the electron energies at which the calculated LEED intensities for the shifted and *ABAB* stackings are largely different.

We showed using LEEM and LEED *I-V* calculations that the shifted stacking appears at the boundary between the *AB*- and *AC*-stacked domains. However, spatial resolutions of LEEM are not high enough to determine the width of the boundary structure with the shifted stacking and the magnitude of the deformation in the carbon-carbon bonds. We therefore used STM to investigate the domain boundary structure in bilayer graphene in more detail. Figure 5 shows DF LEEM and STM images of epitaxial FLG with the average thickness of bilayer. The stacking domains in Fig. 5(a) are much denser than those in Fig. 1. We measured STM images of the boundary between the monolayer and bilayer and discriminated between them from the corrugations induced by the interface $6\sqrt{3}\times 6\sqrt{3}$ structure.[25] Figures 5(c)–5(e) are magnified images of the dotted squares in Fig. 5(b). While dots are arranged in hexagonal patterns in Figs. 5(c) and 5(e), a honeycomb pattern is seen in Fig. 5(d). Figure 5(b) shows that the honeycomb patterns are sandwiched between the hexagonal patterns. The hexagonal patterns are due to the asymmetry between a' and b' sites and specially belong to the *AB*-type stacking. In the shifted stacking, a' and b' sites are in rather similar environments, which could lead to the honeycomb pattern in the STM images. Figure 5(b) shows that the domain boundary, the width of which is roughly indicated by arrows, runs almost vertically. However, the deformation of the carbon-carbon bonds is even beyond the spatial resolution of our STM instrument.

The fact that the domain boundary prefers the shifted stacking rather than *AA* stacking is also supported by *ab initio* total-energy calculation results. Aoki and Amawashi have already calculated changes in the energy of bilayer graphene caused by the shift of the top layer between *AB* and *AC* stackings.[26] They showed that *AB*(*AC*) and *AA* stackings provide the lowest and highest energies, respectively, and that the energy difference between *AB*(*AC*) and shifted stackings is much smaller than that between *AB*(*AC*) and *AA* stackings.[26]

Recently, it has been shown that the 2D band in the Raman spectra of epitaxial graphene is blueshifted compared with that of exfoliated graphene.[27–29] The blueshift indicates that the epitaxial graphene grown on SiC(0001) is compressively stressed, the cause of which is believed to be the difference in the thermal-expansion coefficient between graphene and SiC.[28,29] The stacking domains in bilayer graphene reasonably mean that one layer is stressed with respect to the other layer, which seems consistent with the above Raman result. Linear bumps sometimes appear on the surface of epitaxial FLG,[30] which would indicate that the top layer is compressed with respect to the lower layers. When we hypothetically compress the top layer in bilayer graphene uniformly along the $\vec{a}+\vec{b}$ direction, a stacking similar to the shifted stacking can appear between *AB*-type and *AC*-type stackings. Here, *AB*-type stacking reflects a lattice mismatch between the top and bottom layers. In reality, however, the DF LEEM intensity in each stacking domain is quite uniform and the domain boundaries provide distinct contrasts in the LEEM images. These facts could suggest that the top layer is not uniformly compressed, that is, the lattice mismatch is relieved only near the domain boundaries. This is also consistent with the STM results. The strain energy should increase rapidly with the decrease in the lattice constant. Therefore, uniform compression would minimize the strain energy. However, bilayer graphene energetically favors *AB* and *AC* stackings. The balance between these two energetic factors could lead to the domain structures of *AB* and *AC* stackings.

We do not know the reason for the stacking domains but we suppose the following scenario possible. Even though the starting SiC surface has a regular step/terrace structure, the surface becomes rough during the $\sqrt{3}\times\sqrt{3}$-to-$6\sqrt{3}\times 6\sqrt{3}$ transition in UHV.[9] Graphene preferentially nucleates at the steps.[9,31] We found that the surface flattens during the graphene growth and step/terrace structures somewhat recover regularity after bilayer growth. The topmost graphene is continuous and this layer is grown on a surface rougher

than that of the lower second layer. Wider graphene is necessary to cover a rougher surface. Therefore, the top layer in bilayer graphene is wider in area than the bottom one and the top graphene layer is compressed to match the smoother surface, resulting in the stacking domains. However, an understanding of the detailed growth mechanism of epitaxial graphene is necessary in order to judge the validity of this scenario, and this is a future subject. It could also lead to an explanation of why the stacking domains do not have a strong relationship with the substrate steps.

So far, we proposed that the rough-to-smooth transition of the SiC substrate during graphene growth causes the compression (mismatch) of the top layer in bilayer graphene with respect to the bottom layer, which leads to the stacking domains. However, the analogy of a two-dimensional Ising system may indicate that the coexistence of *AB* and *AC* stackings occurs even in ideal bilayer graphene as a consequence of their energetic degeneracy. In such an ideal situation, we could expect phase-transitionlike behavior where the domain pattern depends on the temperature. The domain pattern observed at room temperature would be the one frozen at a certain high temperature during sample cooling. However, we found that the domain patterns in bilayer graphene remain mostly unchanged after postgrowth annealing even at the temperatures we used to grow the bilayer. The observed stacking domain patterns do not seem to be determined through the phase-transitionlike behavior and we believe that their origin is the mismatch between the two layers. However, this does not always exclude the possibility that ideal bilayer graphene has a domain structure because the bilayer graphene we grew might be far from ideal. To verify the possibility, we need further experimental studies for the growth of more ideal bilayer graphene and also theoretical investigations.

IV. SUMMARY

In this paper, we investigated domain structures of epitaxial bilayer graphene grown on SiC(0001). Dark-field LEEM images and calculated LEED *I-V* curves of (10) and (01) beams indicate that bilayer graphene consists of two types of domains with *AB* and *AC* stackings. We also found that the domain boundaries have a shifted stacking. The stacking domains are also supported by STM images showing graphene has both hexagonal and honeycomb patterns. The domain structures may degrade the electronic transport properties in FLG. We need to understand the formation mechanism and to control the density in order to understand how the stacking domains influence on the electronic transport properties.

ACKNOWLEDGMENTS

This work was partly supported by KAKENHI (Grants No. 19310085 and No. 20340077) from the Ministry of Education, Culture, Sports, Science and Technology of Japan.

[1] A. K. Geim and K. S. Novoselov, Nature Mater. **6**, 183 (2007).
[2] I. Forbeaux, J.-M. Themlin, and J.-M. Debever, Phys. Rev. B **58**, 16396 (1998).
[3] T. Ohta, A. Bostwick, T. Seyller, K. Horn, and E. Rotenberg, Science **313**, 951 (2006).
[4] T. Ohta, A. Bostwick, J. L. McChesney, T. Seyller, K. Horn, and E. Rotenberg, Phys. Rev. Lett. **98**, 206802 (2007).
[5] S. Y. Zhou, G.-H. Gweon, A. V. Fedorov, P. N. First, W. A. de Heer, D.-H. Lee, F. Guinea, A. H. C. Neto, and A. Lanzara, Nature Mater. **6**, 770 (2007).
[6] A. Bostwick, T. Ohta, J. L. McChesney, K. V. Emtsev, T. Seyller, K. Horn, and E. Rotenberg, New J. Phys. **9**, 385 (2007).
[7] K. V. Emtsev, F. Speck, Th. Seyller, L. Ley, and J. D. Riley, Phys. Rev. B **77**, 155303 (2008).
[8] H. Hibino, H. Kageshima, M. Kotsugi, F. Maeda, F.-Z. Guo, and Y. Watanabe, Phys. Rev. B **79**, 125437 (2009).
[9] H. Hibino, H. Kageshima, F. Maeda, M. Nagase, Y. Kobayashi, and H. Yamaguchi, Phys. Rev. B **77**, 075413 (2008).
[10] H. Hibino, H. Kageshima, F. Maeda, M. Nagase, Y. Kobayashi, Y. Kobayashi, and H. Yamaguchi, e-J. Surf. Sci. Nanotechnol. **6**, 107 (2008).
[11] T. Ohta, F. El Gabaly, A. Bostwick, J. L. McChesney, K. V. Emtsev, A. K. Schmid, T. Seyller, K. Horn, and E. Rotenberg, New J. Phys. **10**, 023034 (2008).
[12] C. Virojanadara, M. Syväjarvi, R. Yakimova, L. I. Johansson, A. A. Zakharov, and T. Balasubramanian, Phys. Rev. B **78**, 245403 (2008).
[13] K. V. Emtsev, A. Bostwick, K. Horn, J. Jobst, G. L. Kellogg, L. Ley, J. L. McChesney, T. Ohta, S. A. Reshanov, E. Rotenberg, A. K. Schmid, D. Waldmann, H. B. Weber, and Th. Seyller, Nature Mater. **8**, 203 (2009).
[14] R. M. Tromp and J. B. Hannon, Phys. Rev. Lett. **102**, 106104 (2009).
[15] C. Berger, Z.-M. Song, T.-B. Li, Xuebin Li, A. Y. Ogbazghi, R. Feng, Z.-T. Dai, A. N. Marchenkov, E. H. Conrad, P. N. First, and W. A. de Heer, J. Phys. Chem. B **108**, 19912 (2004).
[16] C. Berger, Z. Song, X. Li, X. Wu, N. Brown, C. Naud, D. Mayou, T. Li, J. Hass, A. N. Marchenkov, E. H. Conrad, P. N. First, and W. A. de Heer, Science **312**, 1191 (2006).
[17] G. Gu, S. Nie, R. M. Feenstra, R. P. Devaty, W. J. Choyke, W. K. Chan, and M. G. Kane, Appl. Phys. Lett. **90**, 253507 (2007).
[18] Y. Q. Wu, P. D. Ye, M. A. Capano, Y. Xuan, Y. Sui, M. Qi, J. A. Cooper, T. Shen, D. Pandey, G. Prakash, and R. Reifenberger, Appl. Phys. Lett. **92**, 092102 (2008).
[19] J. Kedzierski, P.-L. Hsu, P. Healey, P. W. Wyatt, C. L. Keast, M. Sprinkle, C. Berger, and W. A. de Heer, IEEE Trans. Electron Devices **55**, 2078 (2008).
[20] J. Hass, R. Feng, T. Li, X. Li, Z. Zong, W. A. de Heer, P. N. First, E. H. Conrada, C. A. Jeffrey, and C. Berger, Appl. Phys. Lett. **89**, 143106 (2006).
[21] M. A. Van Hove, W. Moritz, H. Over, P. J. Rous, A. Wander, A. Barvieri, N. Materer, U. Starke, and G. A. Somorjai, Surf. Sci. Rep. **19**, 191 (1993).
[22] V. N. Strocov, P. Blaha, H. I. Starnberg, M. Rohlfing, R. Claes-

sen, J.-M. Debever, and J.-M. Themlin, Phys. Rev. B **61**, 4994 (2000).
[23] N. Barrett, E. E. Krasovskii, J.-M. Themlin, and V. N. Strocov, Phys. Rev. B **71**, 035427 (2005).
[24] H. Hibino and Y. Watanabe, Jpn. J. Appl. Phys., Part I **44**, 358 (2005).
[25] P. Lauffer, K. V. Emtsev, R. Graupner, Th. Seyller, L. Ley, S. A. Reshanov, and H. B. Weber, Phys. Rev. B **77**, 155426 (2008).
[26] M. Aoki and H. Amawashi, Solid State Commun. **142**, 123 (2007).
[27] Z. H. Ni, W. Chen, X. F. Fan, J. L. Kuo, T. Yu, A. T. S. Wee, and Z. X. Shen, Phys. Rev. B **77**, 115416 (2008).
[28] J. Röhrl, M. Hundhausen, K. V. Emtsev, Th. Seyller, R. Graupner, and L. Ley, Appl. Phys. Lett. **92**, 201918 (2008).
[29] N. Ferralis, R. Maboudian, and C. Carraro, Phys. Rev. Lett. **101**, 156801 (2008).
[30] K. Hayashi, S. Mizuno, S. Tanaka, H. Toyoda, H. Tochihara, and I. Suemune, Jpn. J. Appl. Phys., Part II **44**, L803 (2005).
[31] J. B. Hannon and R. M. Tromp, Phys. Rev. B **77**, 241404(R) (2008).